Electrochemical Cathodic Protection Powered by Triboelectric Nanogenerator

Wenxi Guo, Xiaoyi Li, Mengxiao Chen, Lu Xu, Lin Dong, Xia Cao, Wei Tang, Jing Zhu, Changjian Lin, Caofeng Pan,* and Zhong Lin Wang**

Metal corrosion is universal in the nature and the corrosion prevention for metals plays an important role everywhere in national economic development and daily life. Here a disk triboelectric nanogenerator (TENG) with segmental structures is introduced as power source to achieve a special cathodic protection effect for steels. The output transferred charges and short-circuit current density of the TENG achieve 1.41 mC/min and 10.1 mA/m^2, respectively, when the rotating speed is 1000 revolutions per minute (rpm). The cathodic protection potential, Tafel polarization curves and electrochemical impedance spectra (EIS) measurements are measured to evaluate the corrosion protection effect for the 403 stainless steel (403SS). The cathodic protection potential range from –320 mV to –5320 mV is achieved by changing rotation speeds and external resistance when the steel is coupled in a 0.5 M NaCl solution to the negative pole of the disk TENG. The corrosion tests results indicate that the TENG can produce 59.1% degree of protection for Q235 steels in 0.5 M NaCl solution. Furthermore, an application of marine corrosion prevention is presented by mounting the TENG onto a buoy. This work demonstrates a versatile, cost-effect and self-powered system to scavenging mechanical energy from environment, leading to effectively protect the metal corrosion without additional power sources.

1. Introduction

Searching for novel and cost-effective methods to protect the metals from corrosion is significant meaningful in our daily life.[1] So far, various surface treatments and coating techniques have been developed for improving the corrosion resistance of different metals.[2] Cathodic protection (CP) is recognized as one of the most effective ways to protect the metals from corrosion in chloride ions solution.[3] Generally, there are two typical CP systems, the first type is the sacrificial anode cathodic protection (SACP) system in which the steel is electrically connected to a sacrificial anode. The second type is the impressed current cathodic protection (ICCP) system in which the steel is protected by cathodic current from an external power source.[4] For the ICCP system, external power sources, which are required to provide sufficient output, need to be replaced over a period of time, resulting in very high cost and environmental pollutions. As for the SACP system, more active metals are sacrificed to protect the steels from corrosion, and what is more, the protected area is limited to the size of the sacrificed metal. Recent years, a new type of cathodic protection system, photogenerated cathode protection, had been developed by coupling a semiconductor photoanode with a steel electrode, and indicated that the open-circuit voltage of the metals can be shifted to negative values when it was coupled with an UV-illuminated TiO_2 photoanode.[1a,5] However, ultraviolet light source is required in this system. Therefore, an ideal CP system is a sustainable self-sufficient (or self-powered) system that can easily harvest available energy from environment, leading to effectively metal protection without additional power source.

In this paper, we introduce a disk triboelectric nanogenerator (TENG) with segmental structures as the power source to achieve a self-powered cathodic protection for stainless steels by harvesting mechanical energy from our living environment. The output transferred charges and short-circuit current density of the TENG achieved 0.70 C/min and 10.1 mA/m^2, respectively, when the rotating speed is 1000 rpm. When we coupled the 403SS in a 0.5 M NaCl solution to the negative pole of the disk TENG, the cathodic polarization potentials ranging from –320 mV to –5320 mV were achieved by changing rotation speeds and external resistances. The corrosion tests results indicated that the TENG could produce 59.1% degree of protection for Q235 steels in 0.5 M NaCl solution. This work not only demonstrates a highly simple fabrication, strong performance and cost-effect approach to protect 403SS from corrosion, but also develops a new pulse cathodic protection technique that is

W. Guo, X. Li, M. Chen, L. Dong, X. Cao, W. Tang, Prof. C. Pan, Prof. Z. L. Wang
Beijing Institute of Nanoenergy and Nanosystems
Chinese Academy of Sciences
Beijing, China
E-mail: cfpan@binn.cas.cn; zlwang@gatech.edu
W. Guo, L. Xu, Prof. C. Lin
State Key Laboratory of Physical Chemistry of Solid Surfaces
College of Chemistry and Chemical Engineering
Xiamen University
Xiamen 361005, China
E-mail: cjlin@xmu.edu.cn
X. Li, Prof. J. Zhu
Beijing National Center for Electron Microscopy
Department of Material Science and Engineering
Tsinghua University
Beijing 100084, P. R. China
Prof. Z. L. Wang
School of Materials Science and Engineering
Georgia Institute of Technology
Atlanta, GA 30332–0245, USA

DOI: 10.1002/adfm.201401168

likely to be widely used in industry, agriculture, transportation and so on.

Recently, TENG has been demonstrated as an effective approach to convert mechanical energy into electricity,[6] with performance depending on the coupling of triboelectrification[7] and electrostatic induction,[6a] through the contact separation or relative sliding between two materials that have opposite tribopolarity.[8a] Compared to the traditional power sources, TENG has the advantages of easy fabrication, excellent durability, high output and low cost.[8] What is more, TENG can easily harvest almost all types of mechanical energy including human activities, wheels moving, mechanical vibration and so on, which is significantly high enough for the widespread metals corrosion protection.

2. Results and Discussion

The structures and working principle of the TENG are shown in **Figure 1**. The basic structure of the TENG is composed of Kapton and aluminum segmentally structured friction disk, as illustrated in Figure 1a. Figures 1b,c are digital images showing the detailed parts of a real kKapton and aluminum friction disks, respectively. Before driven by a motor, the two disks are assembled together to construct a coaxial structure, as shown in Figure 1a. In order to enhance the output of the TENG, a thin layer of Kapton nanorod (NR) arrays was fabricated on the surface to increase the effective contact area between two layers. SEM images of the Kapton nanorod arrays (NRs) after a two-minute ICP etching are presented in Figure 1d,e, it can be found that the NRs are uniformly distributed on the surface of Kapton, with an average diameter of 120 and length of 500 nm, respectively.

According to the previous work reported by Lin et al.,[8a] the working mechanism of disk TENG can be divided into four different processes as shown in Figure 1f. At the beginning, the Kapton and Al films fully contacted with each other (Stage I, Figure 1f) and then surface charge transfer takes place at the contact area due to triboelectric effect,[7,9] resulting in tribocharges were separated at the interface of Al foil and Kapton film. In Stage II, the Al foil slides rotate in reference to the Kapton film, a partially mismatched contact area established an electric potential difference (EPD) between the two electrodes. A higher induced potential on the Al layer will drive the electrons flow from Kapton film to the Al foil through an external load, so that an instantaneous current output corresponds to an opposite potential is generated, as shown in Stage III. Further spinning the top plate, another adjacent sector of Al foil begins to contact with the Kapton film, inversely, the decrease of the mismatch area will decrease the EPD between two electrodes and result in the electrons will flow back in the opposite direction from the Al foil to the electrode attached to the Kapton film, as shown in Stage IV. Thus, an alternating-current (AC) output could be generated periodically when the two plates rotate in reference to each other.

The electrical output of the TENG-430SS system was measured based on a mechanical-electrochemical process. **Figure 2**a shows the structures and working principle of the TENG-403SS cathodic protection system. When the TENG starts to work, the transferred electrons will inject into the steels, resulting in a cathodic polarization of the steels. The current density J_{SC} and the transferred charge quantity ($\Delta\sigma$) were measured by an electrometer (Keithley 6514). The influence of the rotating speeds on the output performance of the disk TENG loaded with the electrolytic cells were measured as well at a rotation speeds of 100 rpm-1000 rpm by using a full-wave rectifying bridge. As shown in Figure 2b, the instantaneously maximum $\Delta\sigma$ peaks are around 59 $\mu C/m^2$ and they are almost keep constant with the rotating speeds increased from 100 rpm to 1000 rpm. The J_{SC} is strongly depended on rotating speeds (Figure 2c), which increases from 3.4 mA/cm^2 to 10.1 mA/cm^2, with the rotating speeds increased from 100 rpm to 1000 rpm. The value of the $\Delta\sigma$ and J_{SC} can be calculated by the following equations:[8a]

$$\Delta\sigma = \frac{\sigma_0 \times \Delta\theta}{\theta_0} \tag{1}$$

$$J_{SC} = \frac{\sigma_0}{\theta_0} \times 2\pi \times \frac{n}{60} \tag{2}$$

where σ, θ and n are charge density, rotating angle and rotating speeds, respectively. σ_0 and θ_0 represent a constant value of σ and the rotating angle from a segment to another adjacent segment, respectively. According to the equations, it can be inferred that the rotating speeds (n) has no effect on the value of $\Delta\sigma$ while the value of J_{SC} shows proportional to the rotating speeds, the tendency of which totally agrees with the experimental results.

To investigate the pulse cathodic protection properties of the TENG device, the open circuit potential (OCP) changes of the 403SS electrode coupled with and without TENG device were measured. **Figure 3**a shows the open circuit potential of 403SS electrode in 0.5 M NaCl solution, the corrosion potential of 403SS stays at –63 mV when the TENG is turned off. The potential of 403SS electrode exhibits a markedly negative shift as soon as the TENG is turned on with a rotating speed of 100 rpm. The cathode potential of 403SS continuously decreased and finally reached about –320 mV, the whole process lasted several minutes which is different from photo-generated cathodic polarization, the slow decline of the cathode potential of 403SS could be attributed to pulse cathodic polarization of 403SS when the electrons generated from TENG injected into 403SS periodically. After turning off the TENG, the potential of 403SS was quick recovery and finally stay at about –109 mV which is a little lower than its corrosion potential. To further ensuring the reproducibility of such cathodic protection effect, three more cycles were performed under the same conditions, showing very good repeatability and stability for our TENG-403SS cathodic protection system.

To further study the relationship between the outputs of the TENG, which depended on the rotating speeds, and the OCP value of the 403SS electrode, the OCP changes of the TENG-403SS cathodic protection system was systematically investigated by changing the rotating speeds of the TENG from 100 rpm to 1000 rpm. The corresponding OCP changes of such TENG-403SS cathodic protection system at different rotating speeds is shown in Figure 3b, and it is obvious that the OCP of

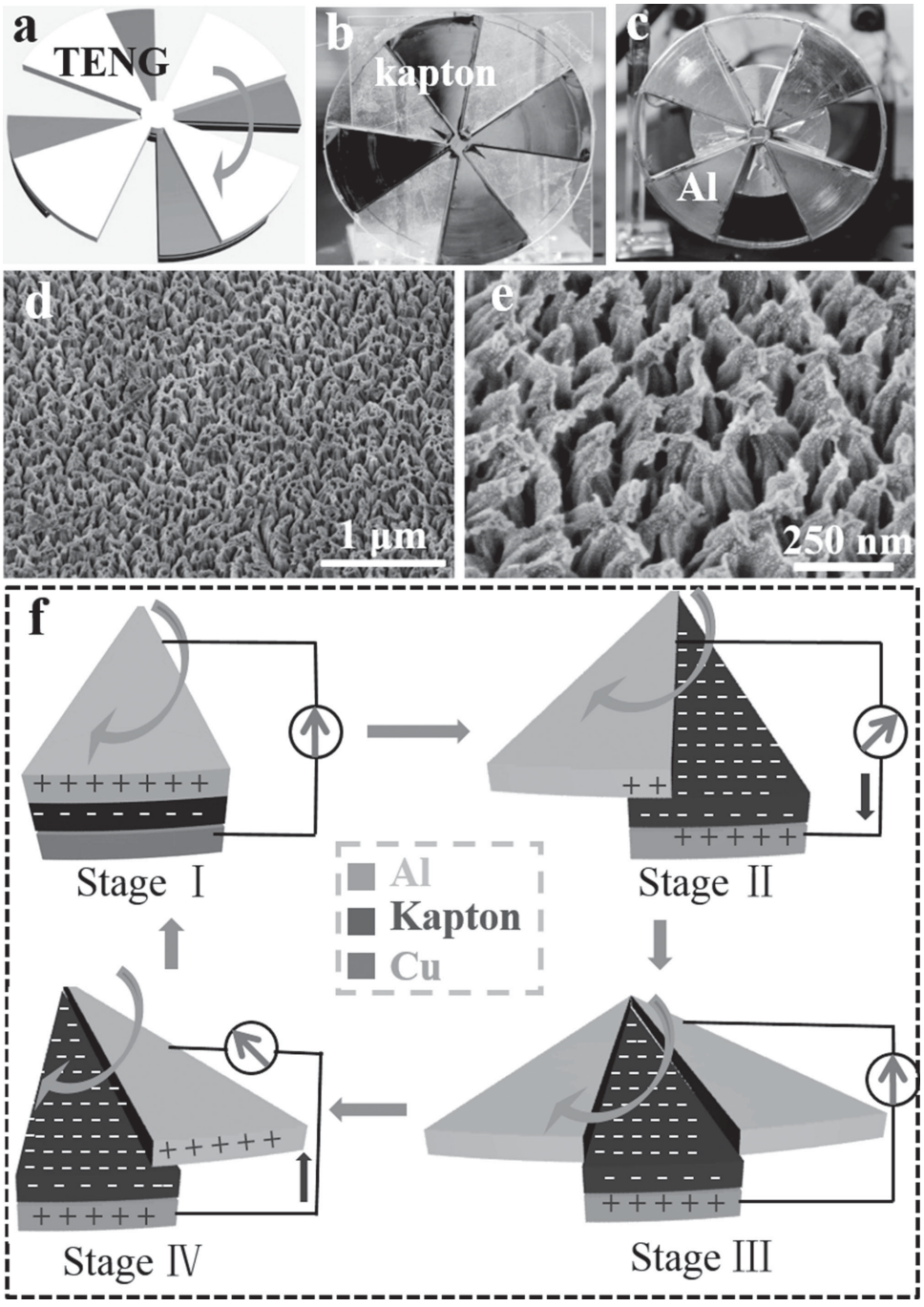

Figure 1. The structures and working principle of the disk TENG. a) A schematic illustration showing the structure design of the disk TENG; b,c) A photograph showing the two parts of a real disk TENG; SEM images of d) a top-view of the Kapton nanorods and e) a high magnification view; f) Schematic illustrations showing the proposed working principle of the disk TENG.

403SS decreased from –330 mV to –440 mV when the rotating speeds increased from 100 rpm to 1000 rpm. The transferred charges and the OCP at different rotating speeds from 100 rpm to 1000 rpm are presented in Figure 3c, obviously, the value of transferred charges is almost proportional to the rotating speeds while the value of the OCP shows the reverse trend. To study the reasons why the OCP value declined when increasing the rotating speeds, the V_{OC} of the TENG loaded with the electrolytic cells at different rotating speeds was evaluated. The relationship between V_{OC} and rotating speeds is shown in Figure S1 (Supporting Information), it is apparent that the V_{OC} almost keep constant when the rotating speeds increased from 100–750 rpm while a decay occurs at the speed of 1000 rpm, which might result from the low sampling acquisition rate of the voltage/charge meter (Keithley 6514 electrometer and Stanford SR570). Accordingly, it is impossible for TENG to bring

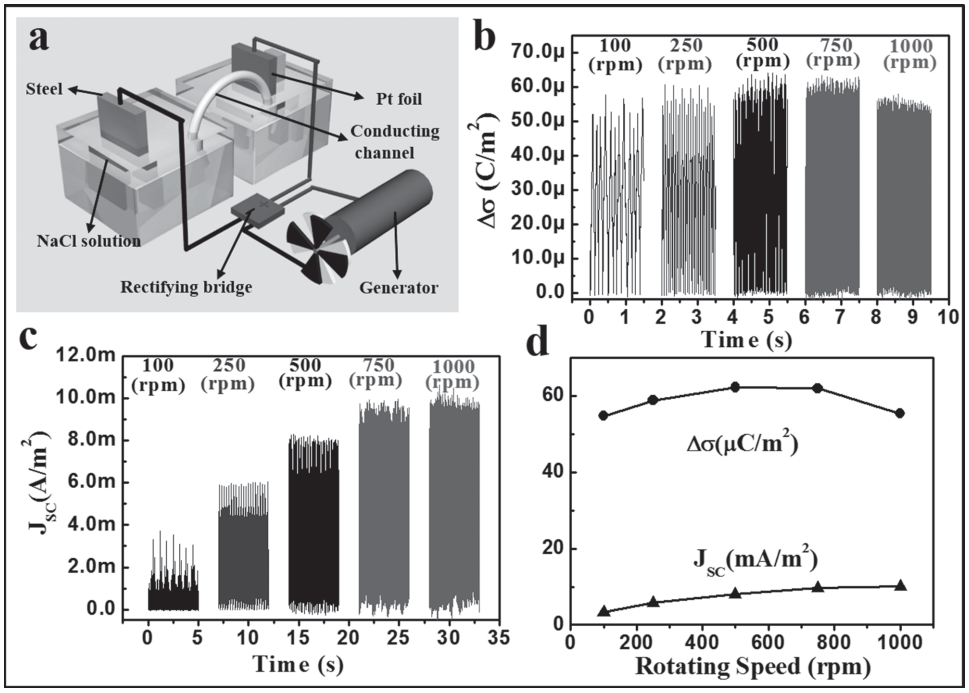

Figure 2. a) The structures and working principle of the TENG-403SS cathodic protection system. a–c) The measured transferred charge density (b), the short-circuit current density (c) and the summarized relationship between the short-circuit current density and the transferred charge density (d) with different rotating speeds from 10 rpm to 1000 rpm, respectively.

down the OCP of the 403SS by increasing the V_{OC} of the TENG. The decline of the OCP of the 403SS should be attributed to the increasing of the transferred charges.

Figure 3d presents the Tafel curves of the TENG-403SS cathodic protection system with different rotating speeds from 0 to 1000 rpm. It is clear that the polarization potential exhibits

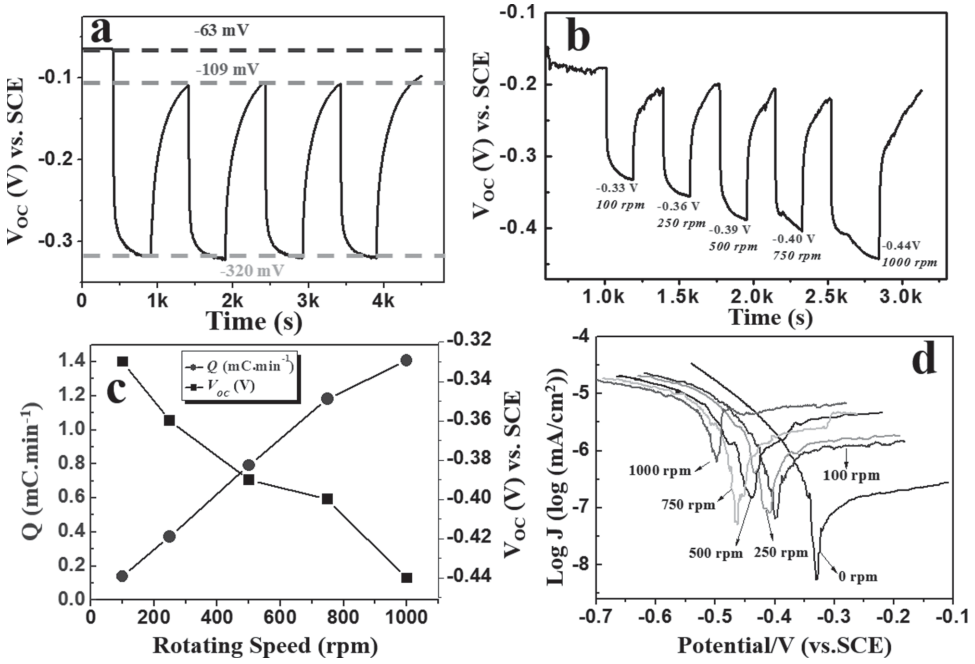

Figure 3. a) The open circuit potential changes of a pure 403SS electrode coupled with and without TENG, the rotating speed of the TENG is 100 rpm; b) The open circuit potential changes of a pure 403SS electrode coupled with TENG at different rotating speeds; c) The summarized relationship between the transferred charge and the open-circuit voltage with different rotating speeds from 10 rpm to 1000 rpm; d) Tafel curves of pure 403SS electrode, and 403SS coupled with TENG at different rotating speeds from 10 rpm to 1000 rpm.

increasing negative shift potentials with increasing the rotating speeds, which is in good agreement with the result of OCP measurement. As can be seen from Figure 3d, the polarization current density which can be estimated by the intercepts of the anodic and cathodic branches also increased with the rotating speeds, indicating that the polarization of the generated electrons from TENG enhance the electrochemical reaction at the interface of the 403SS.[10]

The electrochemical impedance spectra (EIS) measurements were further carried out to recognize the surface properties of the 403SS in the TENG-403SS steel cathodic protection system. **Figure 4**a shows Nyquist plots of the 403SS electrode coupled with TENG at different rotating speeds, it is obvious that the radians of the curves increased with the increasing of the rotating speeds, which is due to generated electrons transferred from the TENG to the stainless steel surface would accelerated the charge transfer between the stainless steel and solution interface. The equivalent circuit inserted in the top-left is proposed to fit the Nyquist plots[2c,11], where R_s,R_{ct}, and Q_{dl} represent the solution resistance, the charge transfer resistance and the double-layer capacitance respectively. The fitting results of EIS for the 403SS electrode coupled with TENG with different rotating speeds are presented in **Table 1**. We can found that the R_{ct} values decrease markedly from 2512 to 2.705 KΩ when the rotating speeds of the TENG increase from 100 rpm to 1000 rpm. The lower R_{ct} indicates that the charge transfer became more effective at the 403SS interface. That is to say, the injection of generated electrons to the surface of 403SS increases the value of J_0 ($J_0 = RT/nFR_{ct}$), resulting in the value of R_{ct} decreasing 3 orders of magnitude.[6b] According to the aforementioned discussions, the value of J_0 is inversely proportional to the OCP of 403SS, that is to say, increasing the rotating speeds would both decrease the value of the R_{ct} and OCP of the 403SS.

In a practical application, –440 mV polarization potential is not sufficient to meet the minimum cathodic protection potentials for a wide variety of metals or alloys. According to the guidelines of cathodic protection implementation (BS 7361: Part 1: 1991, as shown in the Table S1), protective potentials range from +600 to –1200 mV are required to protect various metals or alloys in different corrosive environment. There are two approaches for further stepping down of the cathodic protection potentials: one is to increase the output of the TENG such as by increasing the rotating speeds and contact surface area. The other approach is to increase the external loads of the electrolyte to match the internal resistance of the TENG. Figure 4b shows the resistance dependence of both output current density and voltage of a TENG, from 1000 Ω to 5 GΩ. By increasing the load resistance, the output current density decreases while the output voltage shows the reverse trend. According to the power density equation:

$$\frac{P}{A} = UJ \tag{3}$$

where P and A are the output power and surface area of the aluminum or Kapton disk, respectively, U is the voltage and J represents the current density. Obviously, there is a maximum value for the power density by changing the external loads. The corresponding relationship between the power density and the

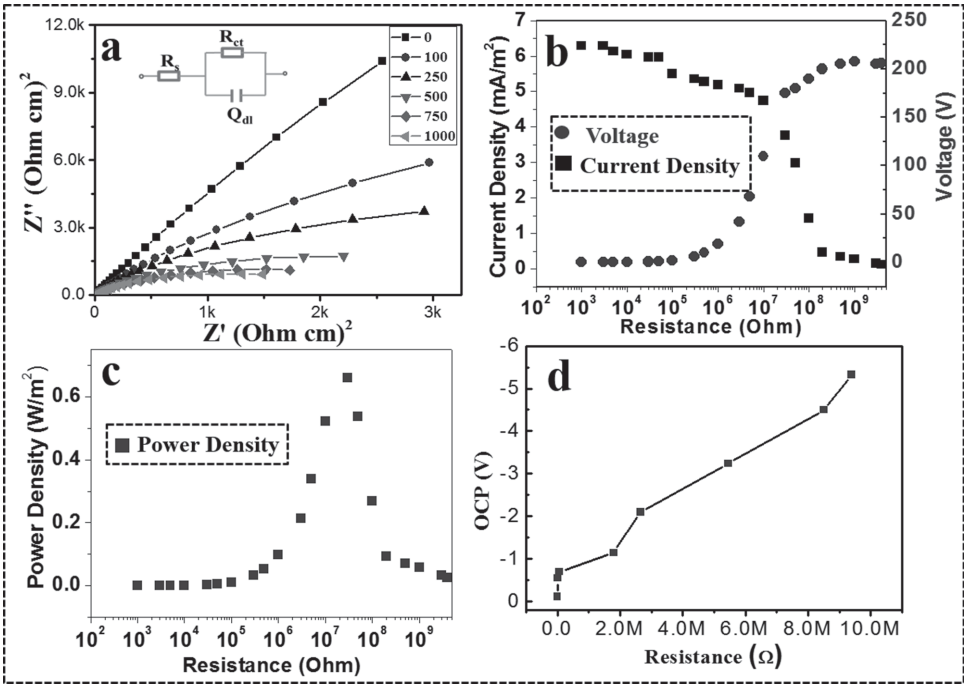

Figure 4. a) Nyquist plots of the TENG-403SS cathodic protection system at different rotating speeds, Z' and Z'' represent the real and imaginary parts of total impedance and they can be defined as: $Z = Z' + Z''_j$; b) Output voltage (right axis) and current density (left axis) as a function of the load resistance; c) Instantaneous power density as a function of the load resistance; d) The measured open-circuit voltage of 403SS as a function of external resistance.

Table 1. The fitting results of EIS for the 403SS electrode coupled with TENG at different rotating speeds.

CEs	R_s [Ω cm^2]	Y_0 [10^{-5} F cm^{-2} S^{n-1}]	n	R_{ct} [kΩ cm^2]
0	7.845	14.13	0.8677	2512
100	7.563	21.78	0.8385	32.05
250	7.506	27.17	0.8262	13.04
500	7.479	37.10	0.8119	5.067
750	7.490	45.45	0.8070	3.242
1000	7.482	50.48	0.8015	2.705

external resistance is presented in Figure 4c, and it is clear that an instantaneous peak value of ≈0.7 W /m^2 at ≈3×10^7 Ω occurs, representing the maximum power density. As a result, the OCP of 403SS in the TENG-403SS cathodic protection system can be tuned by changing the solution resistance. It can be realized by changing the length of the plastic conducting channel between the working electrode and counter electrode, which were placed in two different cells, connected by a capillary filled with 0.5 M NaCl electrolyte. Figure 4d shows the relationship between the OCP of the 403SS and the external resistance when the rotating speed of the TENG was 250 rpm. It is clear that the OCP decreased from –120 mV to –5320 mV when the external solution resistance increased from 3000 Ω to 9.39 MΩ, which is sufficient to meet the minimum cathodic protection potentials for most of the metals and alloys. We note that even lower polarization potential could be obtained if we further increasing the external resistance, however, it is worth nothing to do that due to hydrogen evolution on the surface of the 403SS which would result in over protection.

To confirm the results of the electrochemical measurements, the weight-loss tests of Q235 carbon steel specimens were also performed. **Figure 5** shows the digital photographs of the surface morphology of the Q235 carbon steels powered with TENG and without TENG after immersing in 0.5 M NaCl solution for different time. It is apparent that much more red rust distributed on the surface of the specimen without TENG than that coupled with TENG after one hour of immersion. And in general, once the corrosion spots formed on the Q235 steels, the corrosion rate increased rapidly and abundant rust completely spread across the surface of the Q235 steel as time progressed. When the soaking time was extended to 5 hours, a thick rust film was observed on the partially surface of steel without TENG while still only a few rust at the corner of the steel coupled with TENG, indicating that the TENG can effectively reduce the corrosion rate. To further examine the corrosion state of Q235 steel in NaCl solution with and without TENG, the topographic images of steels after 5 h immersion were observed by SEM as shown in Figure S2 (Supporting Information). Only a few corrosion pits distributed on the surface of the steels with TENG while a thick layer of rust appeared on that without TENG. SEM images (Supporting Information Figure S2b,d) with higher magnification show that the corrosion products were porous and composed by abundant irregular nanosheets. The corresponding EDX spectra as shown in the Supporting Information Figure S2e,f reveal that the corrosion products are mainly composed by Fe, O, and C. It is worth to mention that the corrosion products on the steels without TENG contained much more oxygen than those on the steels coupled with TENG, indicating much less rust was formed on the surface of steels when they were cathodic protected by TENG. The average corrosion rate and degree of protection of the Q235 steels with and without TENG in 0.5 NaCl solution for 5 h were listed in Table S2 (Supporting Information), compared to the steel without TENG, the degrees of protection were 36.4% and 59.1% when the OCP were –0.35 V and –0.85 V, respectively.

Furthermore, TENG can be applied in different corrosion environment according to the different working modes. Here, we present a really application of marine corrosion prevention by mounting the TENG onto a buoy, as shown in **Figure 6**a–c, in which a TENG was built in the vertical contact-separation mode. The TENG was composed by an Al foil with a suspended 3D spiral structure on it and a Kapton film sticking on the

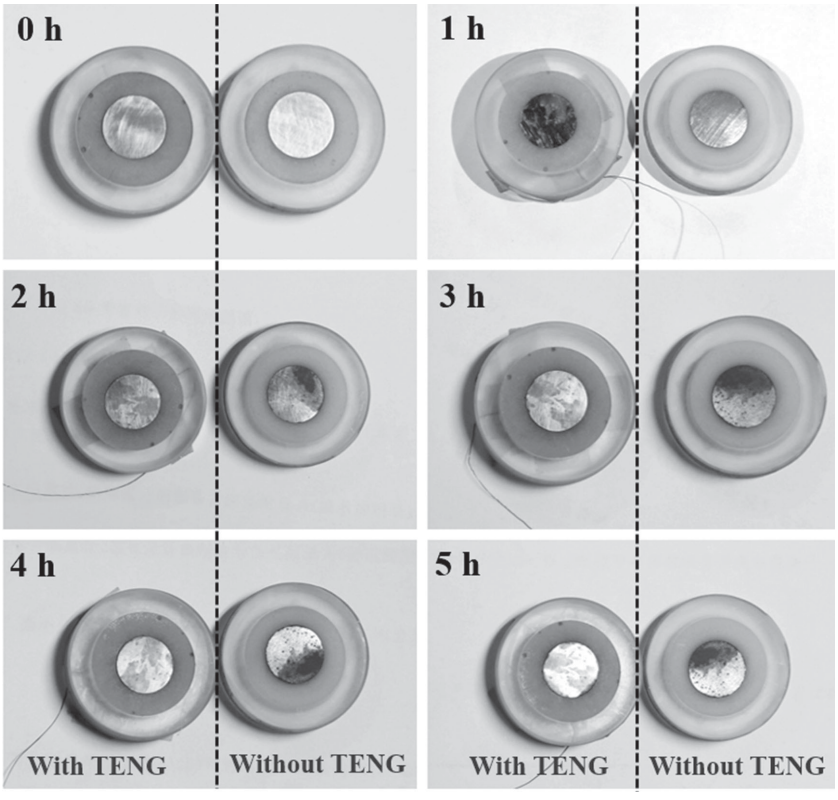

Figure 5. The digital photographs of the surface morphology of Q235 carbon steels after immersing in 0.5 M NaCl solution for different time. The Q235 specimens were separated into two groups, one group specimens (the left ones) were coupled to the negative pole of the disk TENG while the other ones were natural corrosion without any cathodic protection (the right ones).

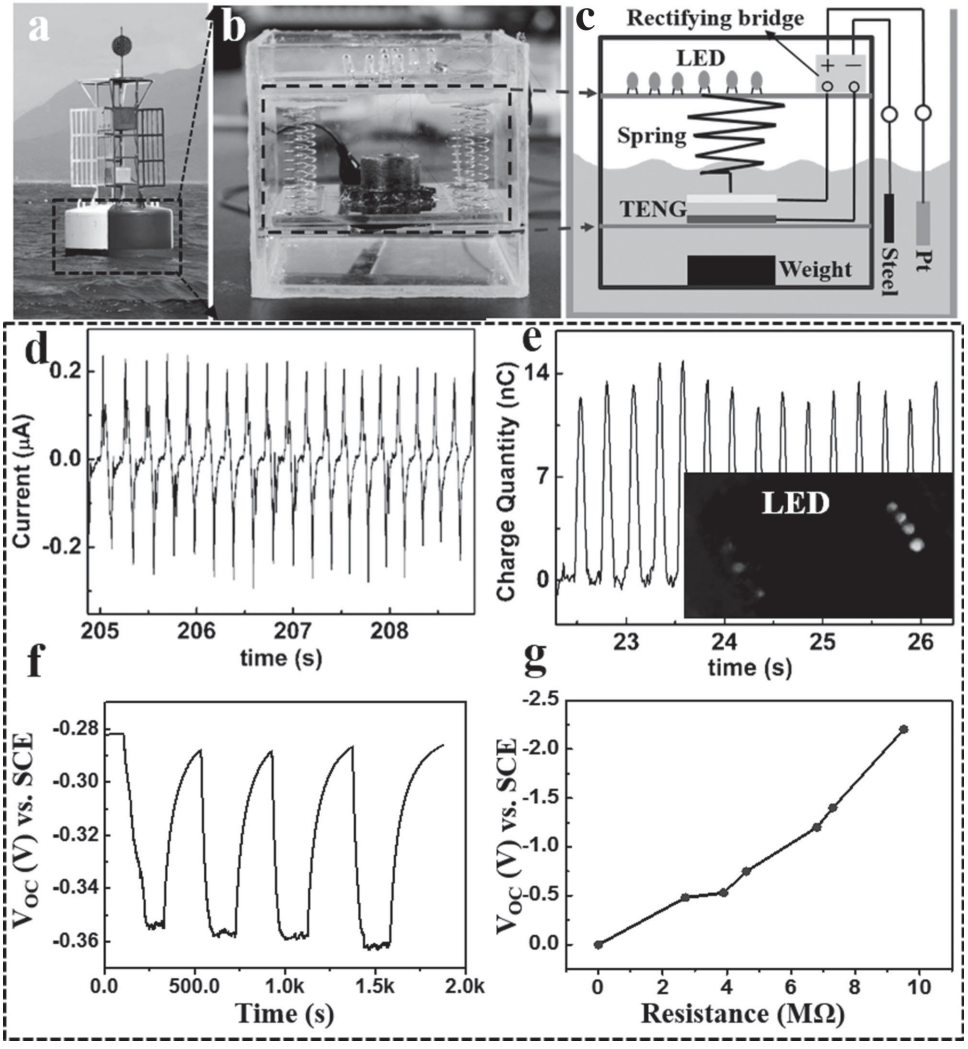

Figure 6. Demonstration of wave energy harvesting and application in marine corrosion protection. a) Taking a smart structure (e.g., a buoy) as a demonstration, the spiral TENG was built into a buoy to harvest the wave energy for self-powered cathodic protection; b) A digital photo of a spiral TENG and c) the corresponding structural representation: the spiral TENG was composed by a Al foil with a suspended 3D spiral structure on it and a kapton film was stuck on the lower part, a weight was stuck on the center of the box as the gravity center to make it float smoothly in the sea water. d,e) Instantaneous current and change quantity, respectively; f) The open circuit potential changes of a pure 403SS electrode coupled with and without TENG; g) The measured open-circuit voltage of 403SS as a function of external resistance.

lower part, a weight was stuck on the center of the box as the gravity center to make it float smoothly in the sea water.[12] With undulating waves, the spring would vibrate up and down and resulted in the two films contacted and separated vertically and periodically. The performances of the spiral TENG were measured in simulative marine environment and the results were shown in Figure 6d,e, instantaneous quantity of electricity of about 13.5 nC and current of 0.2 μA were obtained and such a spiral TENG can driver 8 commercial LEDs by continually shaking the water, as shown in the inset of Figure 6e and the video in the Supporting Information. The corresponding OCP for the spiral TENG-403SS system were measured by coupling the 403SS in a 0.5 M NaCl solution to the negative pole of the TENG, as shown in Figure 6f, and it is obvious that the OCP of 403SS decreased to –360 mV when no additional external resistance was loaded. Figure 6g shows the relationship between the OCP of the 403SS and the external resistance. It is clear that the OCP decreased from –480 mV to –2200 mV when the external solution resistance increased from 2700 Ω to 9.5 MΩ, which is also sufficient to meet the minimum cathodic protection potentials for most of the metals and alloys.

3. Conclusion

In conclusion, we have applied the triboelectric nanogeneraor for electrochemical cathodic protection by harvesting mechanical energy in the environment where the metal is deployed. The disk TENG delivers an open-circuit voltage of ≈310 V and short-circuit current density of 10.1 mA/m^2 with the maximum instantaneous power density of 3.1 W/m^2. A linear relationship is obtained between the short-circuit current density and the

rotation speeds, while the transferred charge quantity nearly has no dependence on it. A self-powered cathodic protection system was firstly built by integrating the 403SS and the disk-TENG. The cathodic protection potential, Tafel polarization curves and EIS measurements were performed, demonstrating that the TENG could produce an extremely efficient cathodic protection for the steels. The cathodic protection potential ranging from –320 mV to –5320 mV was achieved, indicating that the TENG could provide adjustable cathodic protective potentials for corrosion prevention of almost all metals or alloys. The corrosion testing results indicate that the disk TENG could produce 59.1% degree of protection for Q235 carbon in 0.5 M NaCl solution. Furthermore, we presented a really application of marine corrosion prevention by amounting the TENG onto a buoy. This work demonstrates a cost-effective and high performance approach to scavenging mechanical energy from environment, using which a self-powered system is built for effectively protecting the metal from corrosion. This research has potential application in corrosion prevention of equipment without supplying electric power.

4. Experimental Section

Fabrication of the Kapton Nanorods: The Kapton film (140 μm thick) was cleaned with menthol, isopropyl alcohol and deionized water, consecutively. Then it was blown dry with compressed air and deposited a 10 nm Au thin film by sputtering. The inductively coupled plasma (ICP) was used to etch the Kapton to create the nanorods on its surface for one minute. Specifically, the power used to generate a large density of plasma was 500 W, then 100 W was used to accelerate the plasma ions. The flow rate of the flow rate of were 5.0 sccm and 55.0 sccm, respectively. Finnaly, a field emission scanning electron microscopy (FESEM, Hitachi S5500) was ultilized to characterize the Kaption nanorods array.

Fabrication of the Rotating Triboelectric Nanogenerator: The basic structure of the disk TENG was schematically illustrated in Figure 1a–c. The disk TENG include two disk-shaped components with four sectors each. In the fabrication of the TENG, first, two 5 mm-thick PMMA sheets were used as substrates which were obtained by laser cutting machine (PLS6.75, Universal Laser Systems) to form the fans patterns. The tailored Al foil and Kapton film with nanorods (deposited with Cu electrode by sputtering) were finely attached on the PMMA substrates and surfaces were made flat. Then the two cleaned surface (Al and Kapton) were contacted intimately and the Al part was driven to spin on the surface of the Kapton around their common axis. The total effective area of the TENG device is 31.8 cm^2.

Electrical Output Measurement of the Rotating Triboelectric Nanogenerator: In order to measure the electrical output, the Kapton part was secured on a fixed support, while the Al film, which was attached on PMMA substrate, was fixed onto a spinning motor. Please make sure both centers of the two parts were made coincided with the spinning motor's axis. Variable rotating speeds of the Al part could be achieved by tuning the power of the motor. SR570 low noise current amplifier (Stanford Research System) was used to measure the short-circuit current, while Keithley 6514 electrometer was used to measure the open-circuit voltage and transferred charge density.

Electrochemical Characterizations and Measurements: The 403SS sheets (10 mm × 20 mm) were polished by emery papers from grade 600 to 1500 and Al_2O_3 powder with diameters of 1.0 μm and 0.3 μm, and then the obtained sheets were ultrasonically cleaned by acetone, ethanol and deionized water for 10 min, respectively. The open circuit potential (OCP) changes of the 403SS electrode coupled with TENG were performed in a three-electrode experimental system using an autolab electrochemical workstation. A 403SS electrode with an active area of 1 cm^2, a saturated calomel electrode (SCE), and a platinum foil were used as the working electrode, reference electrode, and counter electrode, respectively. The electrolyte for the measurement was 0.5 M NaCl. The autolab electrochemical workstation was used to measure the Tafel polarization curves at a scan rate of 5 mV/s. The autolab model PGSTAT 30 (ECO Chemie B.V.) equipped with Frequency Response Analyze (FRA) module (Autolab, Eco-Chemie,) was employed to record the Electrochemical impedance spectra (EIS). The frequency range from 100 kHz to 0.1 Hz with an ac amplitude of 10 mV was explored.

Weight-Loss Test: The disk-shaped Q235 reinforcement steels used in weight-loss test were sealed with epoxy resin except the working surface of 0.95 cm^2 was exposed. In order to obtain the smooth surface, the reinforcement steels were polished with SiC paper from grade 400 to grade 1500 and then followed by ultrasonically cleaned with acetone and alcohol for 5 min, respectively. The simulated solution for the weight-loss test was 0.5 M NaCl and double deionized water and analytical pure grade reagents were used to prepare all the solutions. The cathodic protective specimens were connected to the negative pole of a disk TENG while the specimens without TENG were just immersed in NaCl solution as comparison. The corroded specimens were brushed by a rubber to remove the rust and then washed by deionized water, ethanol and acetone, respectively. The obtained specimens were dry in an oven and weighed with analytical balance.

Supporting Information

Supporting Information is available from the Wiley Online Library or from the author.

Acknowledgements

W.G., X.L., and M.C. contributed equally to this work. The authors thank for the support from the "thousands talents" program for pioneer researcher and his innovation team, China; President Funding of the Chinese Academy of Sciences, National Natural Science Foundation of China (No.51272238 and 21321062), and Henan Univ. Innovation Talents Project (No.13HASTIT020), and the National Basic Research Program of China (2012CB932900), and the International Scientific and Technological Cooperation of MOST (2014DFG52350).

Received: April 11, 2014
Revised: July 2, 2014
Published online: August 26, 2014

[1] a) H. Park, K. Y. Kim, W. Choi, *Chem. Commun.* **2001**, 281; b) P. A. Kilmartin, L. Trier, G. A. Wright, *Synth. Met.* **2002**, *131*, 99; c) C. Punckt, M. Bolscher, H. H. Rotermund, A. S. Mikhailov, L. Organ, N. Budiansky, J. R. Scully, J. L. Hudson, *Science* **2004**, *305*, 1133; d) G. L. Song, *Adv. Eng. Mater.* **2005**, *7*, 563.

[2] a) R. Bhaskaran, N. Palaniswamy, N. S. Rengaswamy, M. Jayachandran, *Anti-corrosion Methods Mater.* **2005**, *52*, 29; b) R. Singh, N. B. Dahotre, *J. Mater. Sci.: Mater. Med.* **2007**, *18*, 725; c) C. Q. Ye, R. G. Hu, S. G. Dong, X. J. Zhang, R. Q. Hou, R. G. Du, C. J. Lin, J. S. Pan, *J. Electroanal. Chem.* **2013**, *688*, 275.

[3] M. M. S. Cheung, C. Cao, *Constr. Build. Mater.* **2013**, *45*, 199.

[4] a) J. Xu, W. Yao, *Constr. Build. Mater.* **2009**, *23*, 2220; b) S. Yehia, J. Host, *ACI Mater. J.* **2010**, *107*, 577.

[5] a) J. N. Yuan, S. Tsujikawa, *J. Electrochem. Soc.* **1995**, *142*, 3444; b) C. F. Chen, C. H. Shen, C. L. Lin, *Thin Solid Films* **2000**, *377*, 326; c) Y. Ohko, S. Saitoh, T. Tatsuma, A. Fujishima, *J. Electrochem. Soc.* **2001**, *148*, B24; d) H. Yun, C. J. Lin, J. Li, J. R. Wang, H. B. Chen, *Appl. Surf. Sci.* **2008**, *255*, 2113.

[6] a) F. R. Fan, Z. Q. Tian, Z. L. Wang, *Nano Energy* **2012**, *1*, 328; b) G. Zhu, Z. H. Lin, Q. S. Jing, P. Bai, C. F. Pan, Y. Yang, Y. S. Zhou, Z. L. Wang, *Nano Lett.* **2013**, *13*, 847; c) G. Zhu, J. Chen, Y. Liu, P. Bai, Y. S. Zhou, Q. S. Jing, C. F. Pan, Z. L. Wang, *Nano Lett.* **2013**, *13*, 2282; d) Y. S. Zhou, Y. Liu, G. Zhu, Z. H. Lin, C. F. Pan, Q. S. Jing, Z. L. Wang, *Nano Lett.* **2013**, *13*, 2771.

[7] G. S. P. Castle, *J. Electrostatics* **1997**, *40–1*, 13.

[8] a) L. Lin, S. Wang, Y. Xie, Q. Jing, S. Niu, Y. Hu, Z. L. Wang, *Nano Lett.* **2013**, *13*, 2916; b) S. Wang, L. Lin, Y. Xie, Q. Jing, S. Niu, Z. L. Wang, *Nano Lett.* **2013**, *13*, 2226; c) J. Chen, G. Zhu, W. Yang, Q. Jing, P. Bai, Y. Yang, T.-C. Hou, Z. L. Wang, *Adv. Mater.* **2013**, *25*, 6094; d) G. Zhu, C. F. Pan, W. X. Guo, C. Y. Chen, Y. S. Zhou, R. M. Yu, Z. L. Wang, *Nano Lett.* **2012**, *12*, 4960; e) W. M. Du, X. Han, L. Lin, M. X. Chen, X. Y. Li, C. F. Pan, Z. L. Wang, *Adv. Energy Mater.* **2014**, DOI: 10.1002/aenm201301592; f) M. X. Chen, X. Y. Li, L. Lin, W. M. Du, X. Han, J. Zhu, C. F. Pan, Z. L. Wang, *Adv. Funct. Mater.* **2014**, DOI: 10.1002/adfm.201400431; g) Z. L. Wang, G. Zhu, Y. Yang, S. H. Wang, C. F. Pan, *Mater. Today* **2012**, *15*, 532.

[9] a) M. H. Lungu, *Miner. Eng.* **2004**, *17*, 69; b) E. Nemeth, V. Albrecht, G. Schubert, F. Simon, *J. Electrostatics* **2003**, *58*, 3.

[10] G. X. Shen, Y. C. Chen, C. J. Lin, *Thin Solid Films* **2005**, *489*, 130.

[11] J. T. Zhang, J. M. Hu, J. Q. Zhang, C. N. Cao, *Prog. Org. Coat.* **2004**, *49*, 293.

[12] Y. F. Hu, J. Yang, Q. S. Jing, S. M. Niu, W. Z. Wu, Z. L. Wang, *ACS Nano* **2013**, *7*, 10424.